

# Resolving HD 100546 disc in the mid-infrared: Small and asymmetric inner disc inside a bright symmetric edge of the outer disc

Panić, O.<sup>1\*</sup>, Ratzka, Th.<sup>2</sup>, Mulders, G. D.<sup>3,4</sup>, Dominik, C.<sup>3,5</sup>, van Boekel, R.<sup>6</sup>, Henning, Th.<sup>6</sup>, Jaffe, W.<sup>7</sup>, and Min, M.<sup>8,3</sup>

<sup>1</sup>European Southern Observatory, Karl Schwarzschild Strasse 2, D-85748 Garching, Germany  
e-mail: opanic@eso.org

<sup>2</sup>Universitäts-Sternwarte Muenchen, Ludwig-Maximilians-Universität, Scheinerstr. 1, 81679 Muenchen, Germany

<sup>3</sup>Astronomical Institute Anton Pannekoek, University of Amsterdam, Science Park 904, 1098 XH Amsterdam, The Netherlands

<sup>4</sup>SRON Netherlands Institute for Space Research, P.O. Box 800, 9700 AV, Groningen, The Netherlands

<sup>5</sup>Department of Astrophysics / IMAPP, Radboud University Nijmegen, P.O. Box 9010, 6500 GL Nijmegen, the Netherlands

<sup>6</sup>Max-Planck Institute for Astronomy, Königstuhl 17, 69117 Heidelberg, Germany

<sup>7</sup>Leiden Observatory, Leiden University, Niels Bohrweg 2, 2333 CA Leiden, The Netherlands

<sup>8</sup>Astronomical Institute Utrecht, University of Utrecht, PO Box 80000, 3508 TA, Utrecht, The Netherlands

Received; accepted

## ABSTRACT

**Context.** A region of roughly half of the Solar system scale around the star HD 100546 is known to be largely cleared of gas and dust, in contrast to the outer disc extending to about 400 AU. However, some material is observed in the immediate vicinity of the star, called the inner disc. Studying the structure of the inner and the outer disc is a first step to establish the origin of the gap between them and possibly link it to presence of planets.

**Aims.** We answer the question how the dust is distributed within and outside the gap, and constrain the disc geometry.

**Methods.** To discern the inner from the outer disc we use the VLTI interferometer instrument MIDI<sup>\*\*</sup>, and observe the disc in the mid-infrared wavelength regime where disc emission dominates over the star. Our observations exploit the full potential of MIDI, with an effective combination of baselines of the VLTI 1.8 m and of 8.2 m telescopes. With baseline lengths of 40 m our long baseline observations are most sensitive to the inner few AU from the star, and we combine them with observations at shorter, 15 m baselines, to probe emission beyond the gap at up to 20 AU from the star.

**Results.** We derive an upper limit of 0.7 AU for the mid-infrared size of the inner disc, from our longest baseline data. The N-band brightness of the inner disc is not point-symmetric. Our short baseline data place a bright symmetric ring of emission at 11 AU. This is consistent with prior observations of the transition region between the gap and the outer disc, known as the disc wall. The ring inclination and position angles are constrained by our data to  $i = 53 \pm 8^\circ$  and  $PA = 145 \pm 5^\circ$ . These values are close to known estimates of the rim and disc geometry and suggest co-planarity.

**Conclusions.** Micron-sized dust is seen to be distributed asymmetrically in the region from the dust sublimation radius to less than 0.7 AU from HD 100546 in observations from 2004 Jun to 2005 Dec. This small dusty disc is separated from the symmetric edge of the outer disc by a large,  $\approx 10$  AU wide gap cleared of micron-sized dust but possibly populated by larger particles, planetesimals and/or planets. \*\*\*

## 1. Introduction

Gaps and holes are the most prominent and observable features a planet may cause in circumstellar discs (e.g., Paardekooep & Mellema 2004; Crida et al. 2006). These features are observed in a number of young discs using direct imaging in (sub)millimetre and infrared (Piétu et al. 2006; Brown et al. 2009; Thalmann et al. 2010; Andrews et al. 2011; Quanz et al. 2011) or derived indirectly from the observed deficit in the mid-infrared range of the broad-band spectral energy distribution (Calvet et al. 2002; Bouwman et al. 2003; Brown et al. 2007). Photoevaporation or

substellar companions are possible physical processes responsible for gap formation. Although the dynamical influence of embedded bodies has a limited spatial range, gaps and holes in the inner disc can have a major impact on the fraction of stellar light that reaches the outer portions of the disc. Stellar illumination governs the large scale temperature and vertical structure of a disc, and these are, in turn, important parameters in dust evolution and radial migration. Gap structure is therefore crucial both as a direct consequence of orbiting planets and an influential factor for the planet formation process.

A number of known discs around nearby (100-200 pc) young stars possess both substantial inner clearings ( $\approx 10$  AU), and disc material near the star (e.g., Espaillat et al. 2010). The aim of our observations is to spatially resolve dust emission on Solar-system scales from a bright showcase example of these discs, and provide a geometrical characterisation of its gap. The target of our study is the nearby star HD 100546 ( $97 \pm 6$  pc; van Leeuwen 2007). This is one of few objects that have driven the

\* Co-funded by Marie-Curie Actions

\*\* The Mid-infrared Interferometric Instrument of the European Southern Observatory's Very Large Telescope Interferometer.

\*\*\* Based on observations collected at the European Organisation for Astronomical Research in the Southern Hemisphere, Chile; Guaranteed Time VLTI/MIDI observations: 060.A-9224(A), 074.C-0552(A), 076.C-0252(C) and 076.C-0252(F).

research of protoplanetary discs and the link with planet formation over the past decade. The disc around this star has a gap in gas and dust distribution inwards from approximately 10 - 13 AU. This is confirmed by ample observational evidence including both SED modelling and direct observations (Bouwman et al. 2003; Benisty et al. 2010; Tatulli et al. 2011; Mulders et al. 2011; Grady et al. 2005a; Acke & van den Ancker 2006; van der Plas et al. 2009). The hundreds AU large outer disc has been imaged using scattered light observations (Pantin et al. 2000; Augereau et al. 2001; Grady et al. 2005b; Ardila et al. 2007; Quillen 2006), and exhibits a spiral arm structure. The disc has a significant gas reservoir, and emits strong low- and high-excitation CO emission at radii well beyond the inner few tens of AU (Panić et al. 2010; Goto et al. 2012). Because of this, at large scales, the disc around HD 100546 can not be considered as a debris disc but rather a hydrostatically supported viscous gaseous disc similar to discs commonly seen around much younger low- and intermediate-mass stars. With an age of more than 5 Myr (van den Ancker et al. 1997; Guimarães et al. 2006), well beyond the average dispersal timescale in discs (Haisch et al. 2001; Hillenbrand 2008), and with the planet-forming regions severely depleted of material, this disc is more likely to have already formed planets rather than being an active site of ongoing planet formation. These putative planets would have dynamically ‘sculpted’ their physical environment and thus modified or erased the initial conditions in which they had been formed. We therefore regard this disc primarily as a laboratory to study disc-planet interactions.

Study of the inner disc at near-infrared wavelengths allows to locate and characterise the inner rim of the disc, region closest to the star. In Benisty et al. (2010); Tatulli et al. (2011) detailed studies of the inner rim were carried out, placing its location at 0.24 AU. These observations and other prior SED modelling do not, however, provide information on the distribution of colder dust present directly behind the hot rim or inside the gap. To investigate the spatial distribution of the dust in the inner few tens of AU in the disc, we conduct observations of the thermal mid-infrared emission. Mid-IR emission from HD 100546 is bright and extended, as shown by Verhoeff (2009); Liu et al. (2003); Leinert et al. (2004); van Boekel et al. (2004). We use the Very Large Telescope Interferometer (VLTI, Glindemann et al. 2003), and its mid-infrared interferometric instrument (MIDI Leinert et al. 2003). MIDI is used to combine the signal from pairs of 8.2 m unit telescopes (UT-baselines) and 1.8 m auxiliary telescopes (AT-baselines). It provides interferometric data in the spectral range 8-13  $\mu\text{m}$ . With UT-baselines of 40-100 m, the spatial scales of a 1-2 AU are efficiently probed at the distance of nearby star-forming regions of 140 pc. The AT-baselines, on the other hand, offer more flexibility with baselines from 10 m to 200 m, and are highly complementary to the UT-baselines. Observations of discs with MIDI on UT-baselines in the past have provided characterisation of the inner discs around several young stars, e.g., Leinert et al. (2004); Ratzka et al. (2007); di Folco et al. (2009). The possibility to combine these existing data with the shorter AT-baselines, as done in the present work, offers potential to further improve our understanding of the inner disc regions and obtain complementary information about the structure of discs at larger scales.

In Sect. 2 we present our interferometric MIDI data. We assess the data quality and present results regarding the spatial scales and physical regimes probed by these observations. In Sect. 4 we describe our modelling method and our basic physical assumptions. We derive the best fit model. We discuss the constraints on the inner disc size, and investigate the origin of the

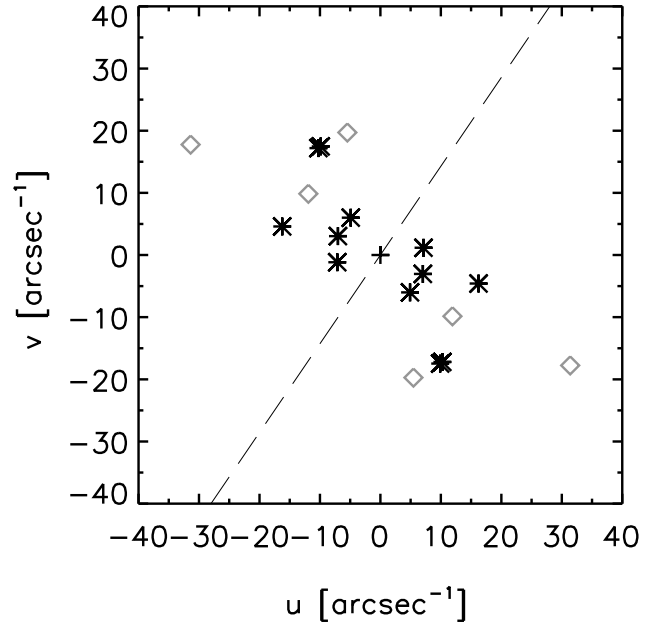


**Fig. 1.** Length and orientation of the baselines corresponding to all MIDI observations HD 100546 taken before 2012. The baselines presented and analysed in this paper are marked by black asterisks. The longest baseline is presented in (Leinert et al. 2004), but the data are not public. The data from the remaining baselines, shown with grey diamonds, is not included either because of poor quality. The orientation of disc major axis used in this work is shown with the dashed line.

observed variability on the 41 m baselines. Section 5 summarises our conclusions.

## 2. Observations and data-reduction

HD 100546 was observed in several campaigns with the two-telescope MID-infrared interferometric Instrument (MIDI) at the Very Large Telescope Interferometer (VLTI). For a detailed description of the instrument and its operation see Leinert et al. (2003); Leinert (2003), Morel et al. (2004), and Ratzka & Leinert (2005). Both the 8-metre Unit Telescopes (UTs) and the 1.8 metre Auxiliary Telescopes (ATs) have been used. A detailed journal of observations is given in Table 1. Figure 1 depicts lengths and orientations of all baselines on which HD 100546 has been observed with the VLTI so far, compared to the orientation of the major axis of the disc. Observations presented in this paper are marked with asterisks.

### 2.1. Observing Sequence

During an interferometric observation with MIDI the spectrally dispersed correlated N-band flux is measured by combining the light from the two telescopes. Two methods are used to suppress background emission: (1) summing the output signals of opposite phase and (2) high-pass time filtering to suppress signals that do not vary at the frequency induced by Optical Path Difference (OPD) scanning (see below). The spectral resolution depends on the dispersive device used during the observation. MIDI offers a prism ( $\lambda/\Delta\lambda \approx 30$ ) and a grism ( $\lambda/\Delta\lambda \approx 230$ ). As seen in Tab. 1 all except one of our observations are obtained using the prism. The piezo-mounted mirrors within MIDI are used to scan

a range in optical path difference (OPD) of typically  $80\mu\text{m}$  in steps of  $2\mu\text{m}$ . At each step, with the corresponding fixed OPD, an exposure is taken to measure the instantaneous value of the interferometric signal. Single frame exposure times were 12 to 18 milliseconds for the prism observations, and 36 milliseconds for the grism observations. Following each scan, the position of the fringe packet in the scan is measured and the VLT delay lines are adjusted accordingly. The scans are repeated typically 200-300 times in saw-tooth manner to increase the statistical accuracy.

Since all the light from the source is used both for the interferometric and then the spectrophotometric measurement, this observing mode is called `HIGH_SENS` mode. Additional non-interferometric photometry was obtained by blocking one telescope after the other while leaving all other optical elements unchanged.

## 2.2. Calibration

The observing sequence described above provides data affected by atmospheric and instrumental correlation losses. To correct for this, the sequence is repeated for a source with known diameter. Ideally the calibrator observation is close to the target observation in time, and in position on the sky, so that the instrumental and atmospheric effects are similar. The instrumental setup, e.g. spectral resolutions, must be identical.

The calibrators are listed in Tab. 1 and have a flux of 5 Jy or more at  $10\mu\text{m}$ . They have no associated circumstellar emission at mid-infrared wavelengths, no close companions nor significant variability. We select several calibrators from the MIDI Calibrator Catalogue<sup>1</sup> and some from CalVin<sup>2</sup>. A subsample of these calibrators, as indicated in Tab. 1, is used for absolute flux calibration<sup>3</sup>. Detailed photometric spectra of these calibrators are taken from a database created by R. van Boekel based ultimately on infrared templates created by Cohen et al. (1999). The details of the construction of the photometric spectra are described in van Boekel (2004); Verhoelst (2005).

The time gap between source and calibrator measurements introduces an uncertainty in the derived fluxes in addition to that arising from noise. In our plots of correlated flux (Figures 4 and 5), the noise uncertainties are indicated by the error bars, while the calibration uncertainties move the spectra as a whole up and down. The magnitude of the calibration uncertainties is indicated in these plots by the black and grey curves, which represent the results derived by two different calibrators. Generally the overall calibration uncertainty of UT observations is  $\sim 10\%$  and of the AT observations  $\sim 20\%$ . We chose the calibrators which allow the AT's total flux spectrum to be consistent with the UT-spectra. The source is slightly resolved in the  $0''.5$  slit of the UTs, as also noted in Leinert et al. (2004). The total field of view of the UTs is approximately  $0.25''$ , that of the ATs is  $2.2''$ . Thus the ATs likely pick up on some additional extended long-wavelength emission from the outer disc regions, and this may explain why there is slightly more flux at long wavelengths seen in the AT's total flux spectra.

## 2.3. Data Reduction

For the data reduction, we use the custom software Version 2.0 of MIA+EWS<sup>4</sup>, written in IDL and the C language. This version is distinguished from the previous ones by an increase in sensitivity due to use of a more sophisticated model of atmospheric time variations in the OPD. Also, there is a reduction of noise bias in weak correlated fluxes.

We chose the EWS branch, which is based on a shift-and-add algorithm in the complex plane. For each frame the atmospheric OPD is estimated from all frames within one atmospheric correlation time, and the phases of the complex visibility of that frame  $A(\lambda) \cdot e^{i\phi(\lambda)}$  are shifted to correct for this OPD. Then all such shifted frames are averaged. Thus, this algorithm is "coherent". For weak sources the OPD determination is most sensitive if the optical path difference (OPD) scan of the interferometric measurements is offset from the white-light fringe (zero OPD), because away from the zero OPD point the interferograms vary rapidly with wavelength, while the sky background does not. For the low spectral resolution of the prism ( $\lambda/\Delta\lambda \approx 30$ ) an offset of about  $5\lambda$  is suitable. However, EWS can also be used safely without an offset from zero OPD when the observed sources are reasonably bright so that the background in no major source of error. Details can be found in Jaffe (2004); Ratzka et al. (2009), and in the documentation on the aforementioned web page. The other branch of the data reduction software, called MIA, analyses the power spectrum. This package works best when OPD scans are centred on zero OPD, but can also handle data tracked at non-zero OPD. The description of the data reduction steps of MIA can be found in Leinert et al. (2004) and Ratzka & Leinert (2005). We here use MIA to confirm the EWS results.

Since we want to model the wavelength-dependent correlated flux  $F_{\text{corr}}(\lambda)$  we calibrate the correlated fluxes directly, approach implemented in EWS. The chosen calibration approach avoids introduction of errors on photometry otherwise imposed when the visibility is calibrated and multiplied by the total calibrated flux to obtain the calibrated correlated flux.

$$F_{\text{corr}}(\lambda) = V(\lambda) \cdot F(\lambda) . \quad (1)$$

The total calibrated flux  $F(\lambda)$  is derived from  $F_{\text{raw}}(\lambda)$  following identical EWS standard procedures for both target and calibrators.

$$F_{\text{corr}}(\lambda) = F_{\text{raw}}(\lambda) \cdot F_{\text{calibrator}}(\lambda) / F_{\text{raw,calibrator}}(\lambda) . \quad (2)$$

## 3. Results

### 3.1. The total N-band fluxes

Previous mid-infrared observations of HD 100546 have been carried out both with the Infrared Space Observatory (ISO) and with ground-based instruments. In Fig. 2 the ISO data (Acke & van den Ancker 2004) are shown. N-band flux of HD 100546 is clearly dominated by a number of spectral features, including a dominant and broad amorphous silicate feature centred at  $9.7\mu\text{m}$ , and somewhat narrower PAH bands atop the silicate feature, at  $7.7$ ,  $8.6$  and  $11.2\mu\text{m}$ . The strong peak near  $11\mu\text{m}$  is due to a blend of PAH and crystalline silicate features. Thorough analyses of the dust spectral features towards our target are presented in Bouwman et al. (2003); Acke & van den Ancker (2004); Mulders et al. (2011). Figure 2 in Bouwman

<sup>1</sup> <http://www.eso.org/~arichich/download/vltcalibs-ws/>

<sup>2</sup> <http://www.eso.org/observing/etc/>

<sup>3</sup> <http://www.eso.org/sci/facilities/paranal/instruments/midi/tools/>

<sup>4</sup> <http://www.strw.leidenuniv.nl/~nevec/MIDI/>

<sup>5</sup> <http://www.mpia-hd.mpg.de/MIDISOFT/>

**Table 1.** Journal of MIDI Observations. Telescopes U2 and U3 are 8.2 m Unit Telescopes, E0 and G0 are 1.8 m Auxiliary Telescopes.

Telescopes / disperser	Date	Universal Time	Time on source [min]	Projected baseline		Calibrators and their N-band fluxes
				[m]	[deg]	
U2-U3 / prism	2004 June 03	01:24-06:50	8	34.8	74.2	HD102461 (9.6 Jy); HD169916* (21.6 Jy); HD120404* (9.3 Jy)
U2-U3 / prism	2004 December 27-28	19:44 - 08:49	10	41.3	30.8	HD219615 (7.9 Jy); 25604 (5.1 Jy); 37160 (6.5 Jy); 98292* (11.9 Jy); 102461* (9.6 Jy)
U2-U3 / grism	2005 December 27	02:45 - 09:00	7	41.4	29.5	HD10380 (9.9 Jy); HD92397 (20.5 Jy); HD112985* (13.1 Jy); HD98292* (11.9 Jy)
E0-G0 / prism	2006 February 13	01:18 - 07:04	10	16.0	39.2	HD44478* (213.3 Jy); HD89388* (33.2 Jy); HD82668 (75.2 Jy); HD61421 (54.8 Jy)
E0-G0 / prism	2006 February 16	03:04 - 06:00	12	15.8	66.6	HD25025 (112.7 Jy); 89388* (33.2 Jy);
E0-G0 / prism	2006 February 16	03:04 - 06:00	12	14.9	99.3	HD25025 (112.7 Jy); 89388* (33.2 Jy);

\* Calibrators used in the data reduction.

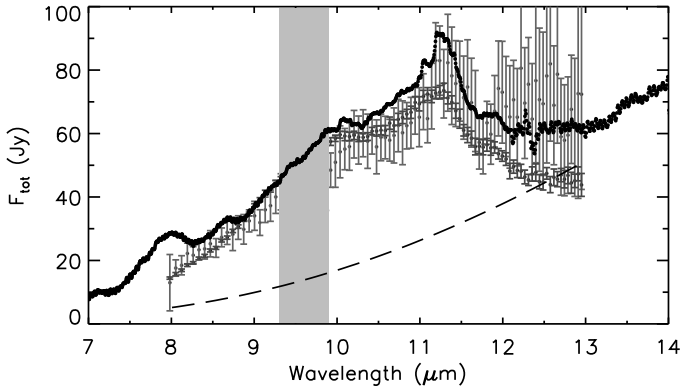


**Fig. 2.** ISO-SWS spectrum from Acke & van den Ancker (2004) is shown in black, a total calibrated flux measurement with an AT (1.8 m) in light grey and with a UT (8.2 m) in dark grey. The dashed line is the prediction from our model described in Sect. 4.3. A masked region from 9.3 to 9.9  $\mu\text{m}$  corresponds to the wavelength range of the atmospheric ozone features affecting our data.

et al. (2003) nicely shows the contributions of different features to the cumulative flux. Our present work focuses on the spatial origin of the emission, and sets aside the complex aspects of dust spectral features, in favour of a more simplistic approach where thermal continuum emission from featureless dust is assumed. In Sect. 4 we will return to our analysis approach in detail.

Our data consists of total N-band fluxes seen by the individual 1.8 and 8.2 m telescopes, as well as the interferometric correlated fluxes obtained with pairs of these telescopes. In comparison with the ISO data, Fig. 2 shows the total calibrated flux measurements from a 1.8 and a 8.2 m telescope. There are some differences, particularly near the PAH 7.7 and 8.6  $\mu\text{m}$  features, and at wavelengths longwards from 10  $\mu\text{m}$ . Total fluxes shown in Fig. 2 are calibrated but not masked, and are therefore limited only by the beam and slit sizes. The slit sizes are  $0''.52$  for UT and  $2''.3$  for AT observations. With neither of our telescopes we fail to recover emission from the aforementioned PAH features. A reason may be the known large spatial extent of the mid-infrared emission towards our target, as studied in great detail in Verhoeff (2009) using VLTi/VISIR observations. Fig. 3 shows their derived deconvolved FWHM sizes of HD 100546 in three wavelength settings across N-band. All PAH features are extended, and in particular, the FWHM of the 7.7  $\mu\text{m}$  feature ex-

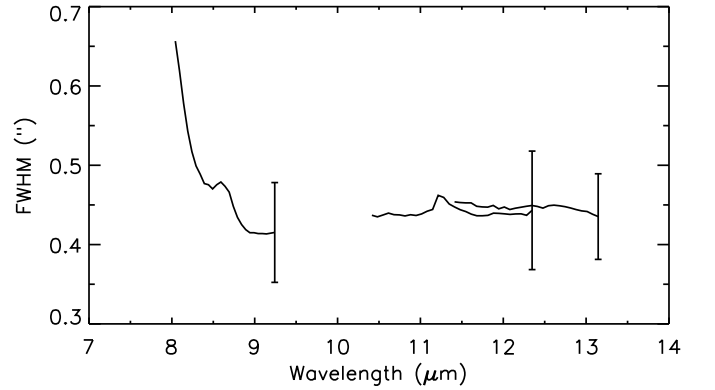


**Fig. 3.** The deconvolved size of HD 100546 as a function of wavelength, derived based on VLT/VISIR observations presented in Verhoeff (2009). Figure adapted from a subplot in Fig. 2.9 of citetverhoeffPhD, Chapter 2. The errors shown at the end of each wavelength setting are medium values.

ceeds the slit size of a UT significantly<sup>6</sup>. Similarly, in their comparison of the total flux measured with a 1.8 m unit telescope to a TIMMI2 measurement, Leinert et al. (2004, their Fig. 2) show that a large fraction of the 8-9  $\mu\text{m}$  flux is not recovered with a UT. The large FWHM of roughly 150 AU was found by van Boekel et al. (2004) for the PAH emission from HD 100546. A further difference between the ISO and our ground based data, at longer wavelengths, is clearly seen in comparison to the data from a 1.8 m telescope. A fraction of the long wavelength flux, originating beyond about 25 AU from the star, is blocked by the slit of  $0''.52$ .

Given the above-mentioned difficulties in our data to probe mid infrared flux from our science target in its entirety due to its large spatial extent, and in particular with some spectral features absent from our data, we do not try to model or analyse the spectral features in this work. For the same reasons, the notion of visibility (correlated divided by total flux) loses its intuitive meaning in case of our target, as its visibilities are strongly influenced by the particular features, and not the underlying continuum emission. For this reason, and because we are primarily interested in the spatial distribution of the dust at small spatial

<sup>6</sup> Based on observations collected at the European Organisation for Astronomical Research in the Southern Hemisphere, Chile; Guaranteed Time VLTi/VISIR observations 075.C-0540A.1

scales, we limit our further analysis to the directly observed correlated fluxes and the total fluxes separately, and not the visibilities.

### 3.2. Interferometric data

A further effect on the angular scales accessible with our observations is introduced by our choice of spatial masks used in the MIDI data reduction. We used the standard masks of the EWS software. This is done to suppress unwanted background emission, and is essential in observations of weak sources. This limits the effective field of view to  $\sim 0.4''$  on the UTs and  $\sim 1.6''$  on the ATs. The comparison between the masked and unmasked N band fluxes measured using UTs shows that masking blocked out less than 10% of the flux. For the ATs the effect is even larger, 25-30%. Our final interferometric data - the correlated fluxes - are therefore derived from a brightness distribution different than the total flux seen with the individual telescopes. We see in Sect. 3.1 that even the total fluxes are affected by the slit size for our bright and extended source. Because of these difficulties, we chose to carry out a comparative analysis of the total and correlated fluxes, instead of the commonly used approach of modelling the visibilities ( $F_{\text{corr}}/F_{\text{tot}}$  directly. Visibilities are widely used in observations of symmetric and radially continuous brightness distributions. However they are not as practical as the fluxes in case of interpretation of data from radially discontinuous gapped distributions like is the case of HD 100546.

The interferometric field of view<sup>7</sup> defines the largest angle on the sky from which coherent light can be combined. For the prism ( $R=30$ ) observations on 41 m baselines it ranges from  $1''.2$  to  $1''.8$  over the N-band wavelengths, while for grism ( $R=230$ ) observations it ranges from  $9''.1$  to  $13''.7$ . On the shorter, 15 m AT baselines (prism), we obtain interferometric fields of view of  $3'' - 6''$ . The angular limitations imposed by the interferometric field of view are therefore not relevant for our data, because these angular scales are much larger than those delimited by the photometric field of view, slit size and masking, discussed in Sect. 3.1.

Figures 4 and 5 show the correlated fluxes  $F_{\text{corr}}$ . We focus on those portions of the mid-infrared spectrum where both the total and correlated fluxes are most likely dominated by the continuum emission from small dust particles. These regions are  $8-9 \mu\text{m}$  and  $12-13 \mu\text{m}$ . At these two wavelengths, the correlated fluxes on the AT baselines are roughly 16% and 23% of the total fluxes. For the UT baselines these percentages are drastically lower: 4-8% and 1-2%. Our calculations show that the situation is very different if a simple continuous brightness distribution from the dust sublimation radius to about 25 AU is assumed. Even when total N-band fluxes are reproduced, such model results in significantly larger flux fractions of about 70% and 46% for the AT baselines and 35% and 20% for the UT baselines. This simple comparison already testifies that the regions of the disc which are well-sampled by our baselines are largely void of dust. Our MIDI data alone thus provide direct and independent evidence that the inner regions of the disc around HD 100546 are severely dust-depleted. This does not hold for very large particles as these do not emit efficiently in the mid-infrared.

The correlated fluxes measured on the UT baselines (Fig. 5) are not only quantitatively, but also qualitatively different from those seen on the AT baselines (Fig. 4). The UT correlated fluxes are comparable across the N-band spectral range, suggesting that

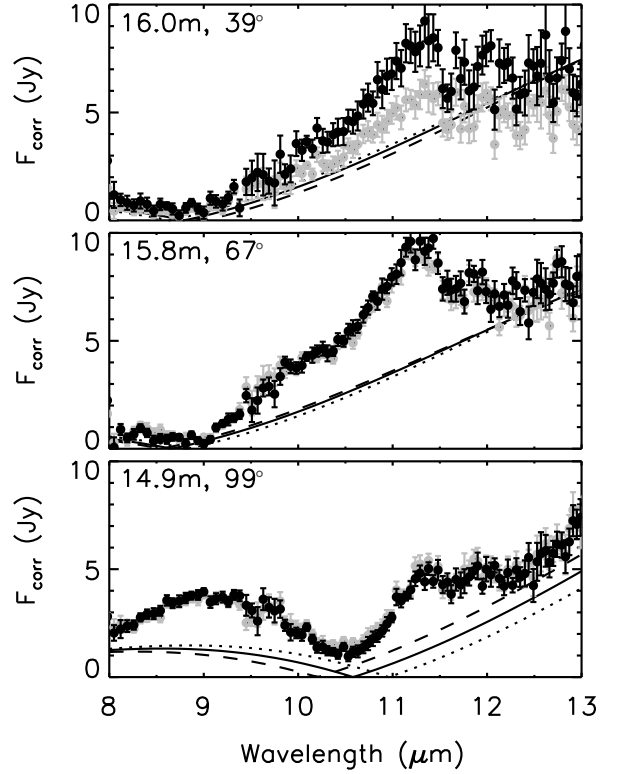


**Fig. 4.** The correlated fluxes obtained with the VLTI auxiliary telescopes in February 2006. Baseline lengths and orientations are indicated. Black and grey symbols correspond to data reduction using two different calibrators, observed immediately prior or following to the science target. The calibration errors are within 20%. The plotted data errors are instrumental errors. Full lines show the model prediction for the correlated fluxes on these baselines (see Sect. 4.3). The dotted and the dashed lines present the model result for position angles  $140^\circ$  and  $150^\circ$  respectively, compared to our model with  $145^\circ$  shown with full lines.

the bulk of this emission arises from relatively hot regions, above a few hundred K. Such temperatures are found in the inner few AU from the star. The AT correlated fluxes, on the other hand, increase towards longer wavelengths, indicating that the dominant emission on these baselines comes from relatively colder material of 200-300 K. These temperatures are found in the outer disc, well beyond the inner few AU.

The spectral shapes of the correlated fluxes measured on the UT baselines are significantly different from one another (Fig. 5, upper panels). In particular, there are two baselines of same length and orientation with significantly different shapes. The only instrumental difference between these two measurements is the spectral resolution (prism vs. grism). The observed variability cannot be in any way related to this, because the variation is present over a spectral range much larger than the channel spacing. The variability is significantly larger than the statistical, instrumental and calibration errors, and cannot arise from any instrumental effects. Therefore it is without any doubt caused by a change in the spatial distribution of N-band brightness toward our science target on the different dates of observation. In comparison to these two baselines, the remaining UT baseline of different geometry has much lower correlated fluxes overall.

<sup>7</sup> The interferometric FoV equals  $R * \lambda / B$ , with  $R$  the spectral resolution and  $B$  the baseline length.

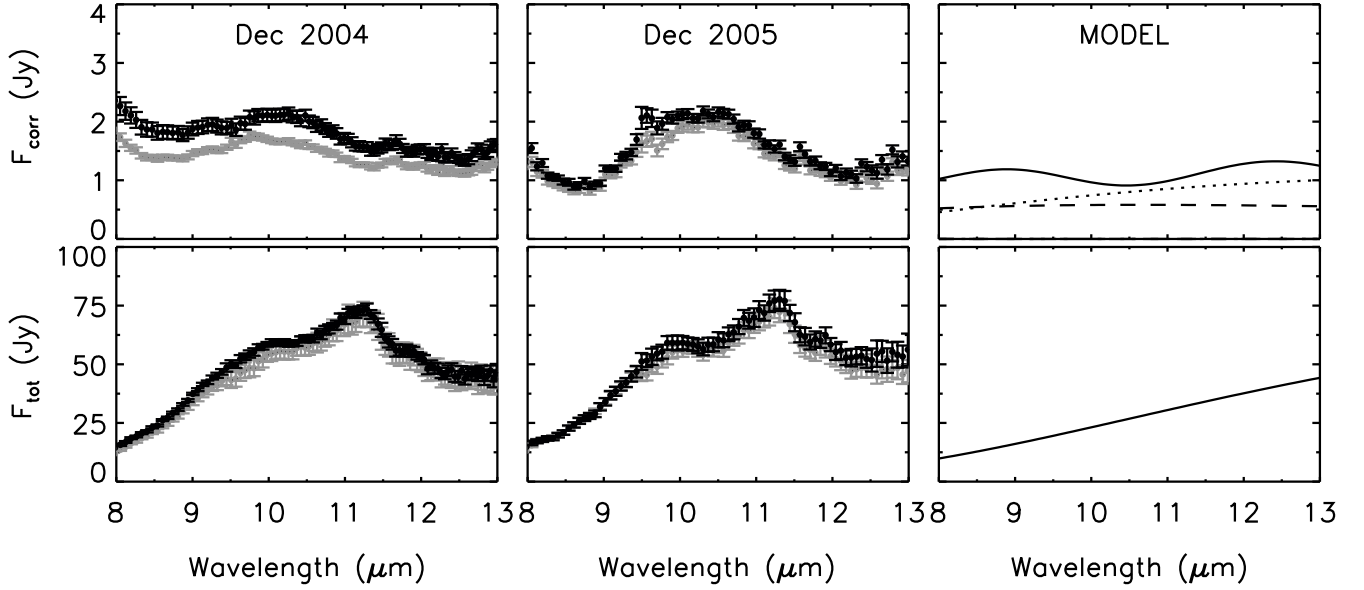


**Fig. 5.** *Upper panels:* The correlated fluxes from UT-baseline measurements observed in December 2004, December 2005 and the modelled correlated fluxes. The baseline length and orientation is 41 m and  $30^\circ$  in both observations. Black and grey symbols are used to distinguish results obtained by using two different calibrators. Error bars correspond to instrumental errors. The dashed and dotted lines show the contribution of the inner rim and the inner disc, respectively. The full line shows the final correlated flux including contributions from all disc components. *Lower panels:* Total unmasked fluxes measured on the unit telescopes simultaneously with the above observations from December 2004 and 2005, and the modelled total flux. As before, black and grey symbols correspond to the use of two different calibrators. Errors shown are due to instrumental errors.

### 3.2.1. Dust spectral features and our interferometric data

As already mentioned in Sect. 3.1, the total fluxes are dominated by a number of spectral features, some of which are extended and therefore not present in all or some of our data. The UT data are especially affected by the slit size and lack some of the short-wavelength PAH features. The only suspected feature seen in our UT correlated fluxes, for example, is a broad and weak bump at 9-12  $\mu\text{m}$  (see Fig. 5, upper panels), which may or may not be related to the silicate feature seen in the total N-band fluxes. A sharp and narrow ring of emission located beyond a few AU from the star can also cause a frequency dependent wavy pattern on the 41 m UT baselines. Because of this, we prefer to focus our analysis on the individual correlated and total fluxes. This allows a better understanding of both, and avoids misinterpretation of the data in terms of spatial distribution. To understand and model the visibilities ( $F_{\text{corr}}/F_{\text{tot}}$ ) directly, is counter-intuitive and extremely difficult in this particular case, and we will not use this approach.

## 4. Discussion

### 4.1. Modelling method

With the set of data that differentially probe the inner and the outer disc, we are able to constrain the size of the inner disc, geometry and location of the bright wall of the outer disc. With the 'disc wall' we hereafter refer to the bright, probably directly illuminated inner edge of the outer disc, located close to 10-13 AU. To analyse our data, we developed an IDL based code which simulates N-band interferometric observations of thermal continuum emission from axially symmetric, vertically flat, disc models. Our models allow for more than one radial component, and is suited to model discs with gaps, like HD 100546. The

calculation of interferometric correlated fluxes relies on the infinitesimal ring approximation. The disc components - the inner and the outer disc - are subdivided in tiny rings from which the correlated fluxes can be calculated analytically, using the aforementioned approximation. The black body emission is attenuated with  $(1 - e^{-\tau})$ , with the dust opacity  $\tau$  either constant, a power law, or allowed to increase radially to simulate the disc wall (explained in later sections).

The main global model parameters:

- $i$  the inclination ( $0^\circ$  corresponds to face-on), constrained by short baselines
- $PA$  disc position angle, major axis measured east of north, constrained by short baselines

The main model parameters for the inner disc are:

- $R_{\text{in},ID}$  the inner radius of the inner disc, fixed
- $R_{\text{out},ID}$  the outer radius of the inner disc, constrained by long baselines
- $T_{ID} = T_{\text{in},ID}(R/R_{\text{in},ID})^{q_{ID}}$  the temperature power law in the inner disc, fixed
- $\tau_{ID}$ , dust opacity in the inner disc, fixed

The main model parameters for the outer disc are:

- $R_{\text{in},OD}$  the inner radius of the outer disc
- $R_{\text{out},OD}$  the outer radius of the outer disc, fixed
- $T_{OD} = T_{\text{in},OD}(R/R_{\text{in},OD})^{q_{OD}}$  the temperature power law in the outer disc, constrained by short baselines
- $\tau_{OD}$ , dust opacity in the outer disc

The parameters  $R_{\text{in},OD}$  and  $\tau_{OD}$  have a single effect of setting the location of the peak brightness of the outer disc wall. These two parameters are degenerate, but rather the only relevant effect of these parameters - the radial location of the peak - is well

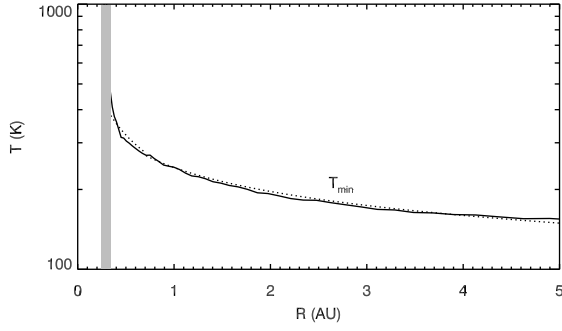


**Fig. 6.** Radial profile of the midplane temperature,  $T_{min}$ , calculated consistently in case where the  $\tau = 1$  surface at  $10.5 \mu\text{m}$  (calculated vertically) coincides with the disc midplane. The dotted line is an analytic fit to  $T_{min}$  (see text). The shaded area is the location of the disc rim.

constrained by our observations and independent observations of the wall of the outer disc, as discussed in Sect. 4.3.

The stellar emission in N-band is negligible with respect to the dust emission, and is added as a point source black body of 10000 K temperature and  $2 R_{\odot}$  diameter. Rim contribution is calculated adopting the rim location of 0.24 AU, outer edge contiguous to the inner disc ( $R_{in,ID}$ ), and temperature  $T_{rim} = T_{in,ID} (R/R_{in,ID})^{q_{rim}}$ . The rim makes a point source contribution on our longest baselines, while it is negligible on our shorter, AT baselines.

There are prominent spectral features in the emission from HD 100546, with different contributions to the total and correlated fluxes due to their differing spatial extents (Sect. 3.1). Because the purpose of our study is not to analyse the spectral features or their extent, but to model the underlying continuum brightness, we limit our work to the analysis and modelling of the correlated and total fluxes, rather than visibilities, as explained in Sect. 3.2. We calibrate the correlated fluxes directly (Sect. 2). The correlated fluxes obtained in this way are more precise, as they are not linked to the photometric errors involved in the acquisition of the total flux. A separate fit to the two observables (correlated and total fluxes) ensures the most efficient exploitation of the information contained in the data. The analysis is more robust than considering visibilities alone, and it is eased by the intuitive link between the model parameters such as temperature and the physical measurements of the total and correlated flux.

#### 4.1.1. Assumptions on the temperature of mid-infrared emitting disc layers

Given the strong effect of the disc temperature on the emerging thermal mid-infrared emission, we investigate several physical scenarios and examine the temperature profile of the  $\tau = 1$  surface at  $10.5 \mu\text{m}$  (centre of N-band). To make rough estimates of possible temperatures, we use a version of the model of Mulders et al. (2011) in which we disregard the gap, and have a continuous radial distribution of disc material from the dust inner radius at 0.24 AU outwards. In the assumptions of the rim temperature we try to keep consistent with the findings of Benisty et al. (2010) and Tatulli et al. (2011), but acknowledge the strong dependence on the yet unconstrained dust properties. We vary the column density to explore several extreme scenarios, and focus on the innermost several AU.

We examine a low density case with the  $10.5 \mu\text{m}$   $\tau = 1$  surface as low as the disc midplane ( $z = 0$ ), and calculate the temperature structure consistently. In this scenario, the mid-infrared emission arises from the lowest possible temperature  $T_{min}$ , the disc midplane temperature, shown in Fig. 6. We obtain roughly  $T_{min} = 235 \text{ K} (R/1\text{AU})^{-0.45}$  between 0.4 and 0.7 AU and  $T_{min} = 242 \text{ K} (R/1\text{AU})^{-0.30}$  between 0.7 and 5.0 AU. Beyond 5.0 AU,  $T_{min}$  flattens off at approximately 150 K. This is by no means the actual temperature dominating the mid-infrared emission of HD 100546, nor does such physical description correspond to the observed mid-infrared fluxes, but it serves as a valuable indication of how low the temperature in these regions may be. To constrain the temperature and derive a three-dimensional disc structure, a sophisticated and full radiative transfer modelling of both SED and existing VLTI data will be presented in a forthcoming paper (Mulders et al. in prep.).

In the present work, we focus on deriving the most robust disc parameters from the MIDI data alone and make simplest assumptions possible. In Sect. 4.2 we assume  $T_{ID}$  to be the disc midplane temperature, and in this way derive an upper limit on the size of the inner disc  $R_{out,ID}$ . In Sect. 4.3 the outer disc temperature  $T_{OD}$  is a free parameter, and derived from our fit to the data. The location where the outer disc begins, and its temperature, are free parameters. However, we try to remain close to the values of 10-13 AU for the disc wall (Bouwman et al. 2003; Quanz et al. 2011), and the physically consistent temperatures in the range 200-300 K, as expected in the case of illuminated wall (Mulders et al. 2011).

#### 4.2. The size of the inner disc

The inner disc regions span a temperature range from few to several hundred Kelvin (see Fig. 6), and emit predominantly in the mid-infrared. The shorter wavelengths are sensitive to even hotter, directly illuminated inner rim of the disc, but such observations (e.g., with AMBER Benisty et al. 2010; Tatulli et al. 2011) cannot constrain the distribution of disc material beyond the rim.

Our interferometric data from 40 m UT baselines are particularly sensitive to the spatial scales of less than a few AU, and we use those correlated fluxes to derive constraints on the spatial structure of the inner disc. The flux contribution from a continuous inner disc to the correlated fluxes is positive and linear. The wall of the outer disc may produce emission at similarly small scales, if the wall is sufficiently narrow and bright. Such features imprint a wavy pattern in the correlated fluxes on the UT baselines. It is precisely because of this possible contribution that we cannot interpret the wavy features seen in correlated spectra in Fig. 5 to dust spectral features.

To make an upper limit on the size of the inner disc, we assume that the mid-infrared flux from this region is emitted at the lowest temperature found in the disc,  $T_{min}$  corresponding to the disc midplane (see Sect. 4.1.1). This temperature profile can be described analytically as a combination of power law slopes:  $T = 235 \text{ K} (R/1\text{AU})^{-0.42}$  between 0.34 and 0.7 AU and a slightly shallower slope  $T = 242 \text{ K} (R/1\text{AU})^{-0.30}$  between 0.7 and 5.0 AU. The temperature from 5 AU until the outer disc wall is roughly 150 K. We assume a continuous transition in temperature from the inner disc to the hot rim, with 370 K at 0.4 AU, to higher values at the innermost radius 0.24 AU (location constrained by AMBER data Benisty et al. 2010; Tatulli et al. 2011). Our only free parameters are therefore the size of the inner disc  $R_{out,ID}$ , and the powerlaw slope of the temperature in the hot rim  $q_{rim}$ .

The correlated flux measurements from Dec 2004 and 2005 are markedly different. Because of this variability (explored further in Sect. 4.4), we only try to make a rough fit to the observed flux levels from 8 to 12  $\mu\text{m}$ , and we focus on fitting the non-variable correlated fluxes at 12–13  $\mu\text{m}$ . This range is free of known spectral features, and we are confident that the flux at these wavelengths is dominated by thermal dust emission.

We obtain an upper limit of  $R_{\text{out,ID}} < 0.7$  AU, and fit the rim temperature  $T_{\text{rim}} = 600 \text{ K } (R/0.24 \text{ AU})^{q_{\text{rim}}}$  with  $q_{\text{rim}} = -1.4$ . Higher temperatures of the rim are possible, but such models yield smaller inner disc sizes  $R_{\text{out,ID}} < 0.7$  AU. The size of 0.7 AU is robust with respect to the temperature of the emitting layer - at higher temperatures the models yield smaller  $R_{\text{out,ID}}$  to compensate for excess flux. In the extreme case, our UT baseline data can even be fit by a rim alone, with an opportune choice of relatively high temperature, near 1000 K. Even higher temperature of the rim, up to 1750 K is used in (Tatulli et al. 2011) to fit the H and K-band emission from HD 100546 observed with AMBER and the near-infrared SED. Combined with such findings, our mid-infrared data imply a minute inner disc, merely a thin ring at the dust sublimation radius.

We also investigate the case of optically thin N-band emission from the inner disc. Again, we assume disc midplane temperatures, but we attenuate the emission by a factor  $1 - e^{-\tau}$ , with a radially dependent optical depth  $\tau = \tau_0 (R/0.4 \text{ AU})^{-1}$ . For simplicity, we neglect the wavelength dependence of the optical depth. We find that in this scenario, the size of the inner disc is not constrained because the flux levels are so low that we no longer can detect any emission beyond 1.5 AU in our observations. A fit to the UT-baseline data is obtained with  $\tau_0 = 0.8$  in N-band. Lower values of optical depth in N-band are ruled out.

It is important to note that the mid-infrared emission is relatively insensitive to large mm and cm-sized particles, and is most sensitive to emission from micron-sized dust. Therefore, any large particles and planetesimals are unconstrained by our data may be more spatially extended than 0.7 AU.

#### 4.3. The model fit

Our MIDI data provide constraints on the spatial distribution of the N-band emission from HD 100546, including the position angle and inclination of the disc. The brightness profile is related to the disc radial temperature structure, and our fit parameters can be used as zeroth-order model for further detailed and consistent physical modelling with sophisticated radiative transfer codes. In this Section, we use the model of the rim and inner disc derived in Sect. 4.2, with low, midplane temperature, and  $R_{\text{out,ID}} = 0.7$  AU as a starting point. The AT baselines are relatively insensitive to the inner disc and do not provide further constraints on this component. Instead, they probe larger spatial scales where strong emission from extended colder material dominates with about ten times larger fluxes ( $\approx 10 \text{ Jy}$  vs  $1 \text{ Jy}$  from the inner disc). We add an outer disc component to the model consisting of the rim and the inner disc. This is needed to fit the fluxes observed on the AT baselines and dominated by relatively colder material. Our AT data thus allows us to characterise the outer disc, and this characterisation is completely independent of the rim and inner disc parameters. For the outer disc, the N-band optical depth is set to  $\tau = 1$  except in the inner parts of the outer disc. To avoid spurious interferometric signal from a high contrast in the flux, we use a taper that simulates a transition from zero density and optical depth to a high density and optical depth of unity. We do this by assigning to  $\tau$  values of a sine function in the dominion  $[0, \pi/2]$  over a spatial range of 8 AU. The effects of

the radial increase in optical depth and decrease in temperature gives rise to a peak of the flux at some radius within the transition region. The peak can be mathematically constructed in a number of different ways, but the exact approach is not relevant in our modelling. The only relevant information is the net result of this approach: a bright peak near 10–13 AU from the star and a smooth transition of flux around the peak.

A prominent feature in each correlated flux measurement shown in Fig. 4 is the presence of a minimum. Each ringlet of brightness in the outer disc contributes to these correlated flux with a wavy pattern across the N-band spectral range. In case of a continuous and smoothly varying radial brightness, the contributions of many ringlets evens out over the spectral range and no prominent minima are expected in the observed correlated fluxes. The fact that we do observe minima in all our short (15–16 m) baselines, unequivocally indicate a dominant spatial feature in the N-band brightness, at scales three times larger than the scales probed by our long (40–42 m) baselines. Based on solid observational evidence for presence of a bright wall close to 13 AU, possibly being a directly illuminated edge of the outer disc, we proceed our analysis with an outer disc model with strong emission in the neighbourhood of 13 AU, and a gradual decrease of disc brightness, consistent with the deconvolved FWHM of  $0''.45$  observed with VLT/VISIR (Verhoeff 2009). The presence of a bright wall has effects on the long baseline data adding a wavy component. Setting a requirement to have comparable correlated fluxes at 8 and at 13  $\mu\text{m}$  on the 40 m baselines (Fig. 5), we obtain  $R = 11$  AU for the peak N-band brightness. Peak locations at 1 AU away from this location are excluded as they are strongly inconsistent with the principal characteristics of the 40 m baseline data. Starting with this basic radial distribution, we vary the disc inclination, position angle and temperature power-law to fit the data.

First we make some considerations, to better understand the dependence of the minima on our model parameters in the context of a axisymmetric disc model as outlined above. For a face-on disc, the only difference between the location of the minima is due to the differences in length between individual baselines. In our case the difference is relatively small, about 1 m and introduces a minor effect in shifting the minimum of the 15 m baseline with respect to the 16 m baselines by less than  $0.8 \mu\text{m}$  towards shorter wavelengths. With increasing disc inclination, the minima of the baselines oriented closest to the minor axis move rapidly to the shorter baselines, and those near the major axis lag behind, as the difference induced by inclination along directions near disc major axis is minimal. Therefore, from the location of the minima of baselines near the minor axis of the disc, and from the comparison to baselines oriented further from the minor axis, we can constrain the inclination and position angle of our science target. In our set of AT measurements, we have three baselines almost evenly spaced with about  $30^\circ$  from one another, as seen in Fig. 1. The strength of correlated fluxes away from the minima (e.g., near 13  $\mu\text{m}$ ) depend on the brightness of the ringlike feature, in our case the disc wall near 11 AU and, to a lesser degree, the radial decrease of disc brightness.

The fact that the two baselines shown in upper and middle panels of Fig. 4 have almost identical correlated fluxes is strongly suggestive of their similar orientation with respect to the disc minor axis. Any baseline length effects can be excluded due to their essentially same length (16.0 and 15.8 m). Setting the minor axis between these two baselines, at  $PA = 145^\circ$  we optimise the fit to the inclination and obtain an inclination of  $i = 53^\circ$ . Setting a conservative  $0.5 \mu\text{m}$  tolerance for the location of the minima, our derived values are  $PA = 145^\circ \pm 5^\circ$  and  $i = 53^\circ \pm 8^\circ$  ( $0^\circ$



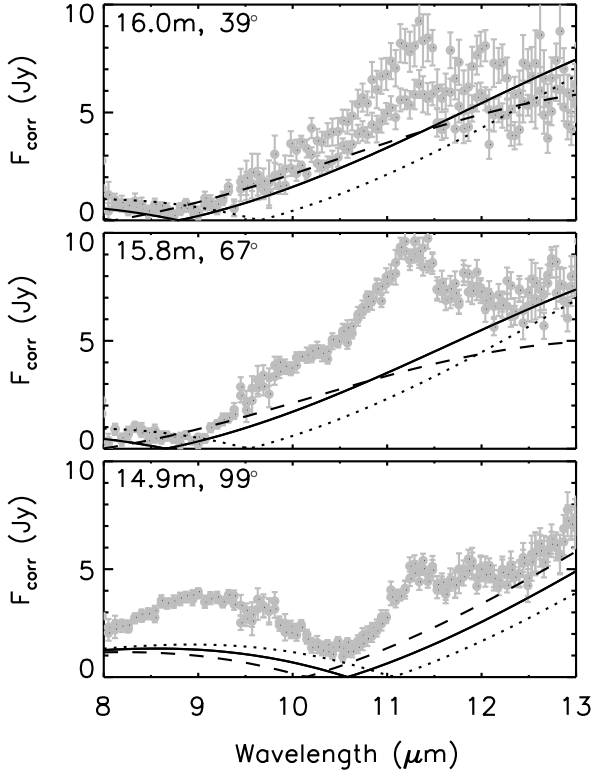


**Fig. 7.** Same data as in Fig. 4, but plotted in grey for both calibrations. Full lines show the model prediction for the correlated fluxes on these baselines (see Sect. 4.3). The dotted and the dashed lines present the model result for inclination angles  $45^\circ$  and  $61^\circ$  respectively, compared to our model with  $53^\circ$  shown with full lines.

corresponds to face-on). The dashed and dotted lines of Fig. 4 show how the results from this model vary depending on the position angle, and Fig. 7 shows the effect of varying inclination angle.

Finally, with the minima and relative 8 and  $13\ \mu\text{m}$  fluxes at levels consistent with our interferometric data, we adjust the temperature in the outer disc to match the high  $13\ \mu\text{m}$  fluxes and low  $8\ \mu\text{m}$  fluxes of the short baselines. The fit is obtained for  $T_{\text{outerdisc}} = 230\ \text{K}(R/9.3\ \text{AU})^{-0.5}$ . With this disc model we match the total fluxes at  $13\ \mu\text{m}$  of  $\approx 50\ \text{Jy}$ , as seen in Fig. 5, but fail to match the  $8\ \mu\text{m}$  fluxes. We explore a range of temperatures and radial distributions of disc brightness, and find that there is a large apparent inconsistency at  $8\ \mu\text{m}$  between the correlated flux levels observed interferometrically and the total flux levels at short wavelengths. A possible scenario is that the excess emission is due to a long wavelength wing of PAH bands centred at  $7.7\text{--}7.9\ \mu\text{m}$ , which, as we find in Sect. 3.1, come from a region larger than the UT slit size of  $0''.52$ .

#### 4.4. Variability of the correlated fluxes

As discussed in Sect. 3.2, there is a significant difference between the two UT baselines of same length and orientation. This is shown explicitly in Fig. 5 where the two baselines are compared. We establish that no instrumental effects play a role here, and the difference persists independently of our choice of calibrator. Therefore the variability we observe in the correlated fluxes implies that in December 2004 and 2005 the spatial distribution of the brightness of the inner disc was different. Although

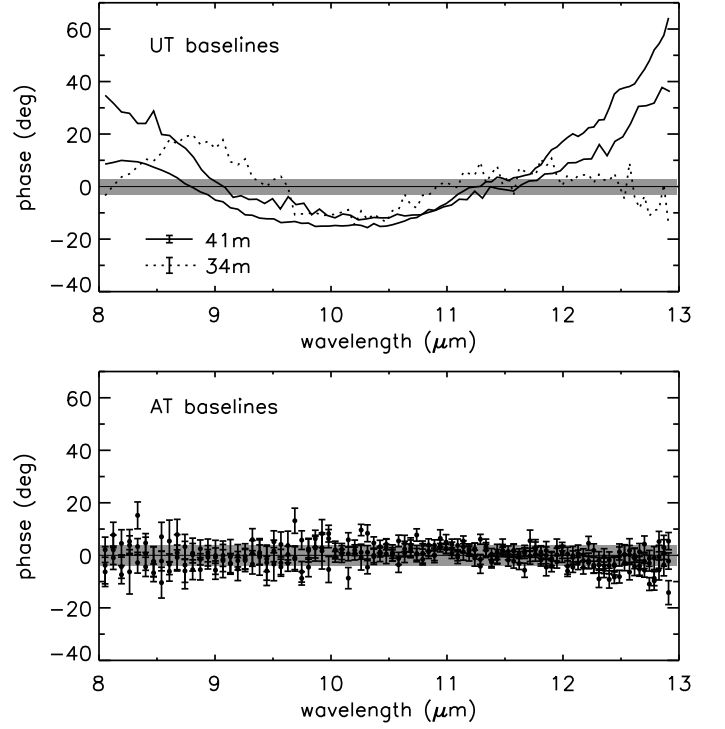


**Fig. 8.** *Top panel:* Calibrated chromatic phases of our UT baseline measurements. The 34 m baselines is plotted with dotted, and 41 m baselines with full lines. Respective errors of  $3.8^\circ$  and  $3.2^\circ$  for these baselines are indicated. Also shown are the zero phases, as predicted from our axially symmetric model. The grey area represents the  $\pm 3^\circ$  tolerance for deviation from zero. A linear, atmospheric term, has been subtracted from the shown phases. *Bottom panel:* As above, for all our AT baselines and axially symmetric model prediction with  $\pm 4^\circ$  tolerance.

it is not possible to reconstruct the image of the inner disc using our data, it is possible to discern between: a) a radial change in brightness of an axially symmetric inner disc and b) a change of the orientation of an asymmetric inner disc with respect to the projected baseline. In the first case, the variability originates due to physical processes that restructure the disc on the timescale of one year (time between the observations). Considering the orbital timescale around a  $2.4\ M_\odot$  star, this scenario is only plausible for processes affecting regions closer than  $1.3\ \text{AU}$  from the star. In view of our conclusions from Sect. 4.2, the inner disc is entirely contained in this region. Considering that the difference is pronounced at short wavelengths while the  $13\ \mu\text{m}$  flux remains constant suggests that the suspected structural changes happen in the directly illuminated hot rim of the inner disc. In the second case, the disc structure does not undergo any changes which may affect the mid-infrared brightness, but is intrinsically asymmetric with respect to the star. Therefore, one year apart, the orientation of such asymmetric feature with respect to our 41 m and  $30^\circ$  baseline is different due to disc rotation, giving rise to different correlated flux measurements nonetheless the physical structure of the source remains unchanged. At scales of roughly  $1\ \text{AU}$  or less the orbital period is less than 1 year, and this is a plausible explanation.

The asymmetric brightness scenario can be tested by the chromatic phase measurements. In case of deviations from point-symmetry, the phases exhibit a deviation from zero, as contributions from opposite sides of the star fail to cancel one another

completely. Axially symmetric disc models, such as ours, necessarily result in zero-phases. Fig. 8 shows the calibrated chromatic phases of our UT baseline measurements, including the 34 m baseline from 2004 Jun. Deviations as large as  $60^\circ$  can be seen. The precision of these measurements was estimated by cross-calibrating pairs of calibrators and comparing the phase difference for each pair. In this way, we find that the chromatic phases are correct to better than  $3.2^\circ$  for the 41 m baselines and  $3.8^\circ$  for the 34 m baseline. Therefore our data presents clear evidence of a lack of point symmetry in the brightness distribution on spatial scales of less than 1 AU in the disc around HD 100546. Combined with our result that the UT baselines are dominated by the dust in the inner disc, we conclude that an asymmetry in the spatial distribution of small dust is present within 0.7 AU from the star. Asymmetry persists in our data from 2004 Jun to 2005 Dec, but we cannot assess if the asymmetry remained the same, rotated, or changed, from one observation date to another. Our short baseline AT data do not show deviations from zero phases, and we therefore do not find evidence for asymmetry in the N-band brightness of the disc wall at 11 AU (see Fig. 8, lower panel).

## 5. Summary

In this work we revisit the bright disc around the intermediate-mass star HD 100546. Although plenty of observational data are available for this source, the physical conditions of dust in the areas adjacent to the gap in the planet-forming regions of this disc are poorly determined. To address this, we take advantage of the VLTI and its ability to observe discs around young stars in a span of spatial scales ranging from the Earth's orbit to the orbit of Uranus. Especially in gapped discs like HD 100546, only interferometric observations can measure and study the flux arising from a relatively small inner disc near the star, separately from the overwhelming outer disc emission at larger scales. The mid-infrared wavelength range covered by the VLTI instrument MIDI is multiply advantageous: the emission is dominated by the disc while stellar contribution is negligible, and the thermal emission of the disc regions of interest is the strongest in mid-infrared, due to the temperature range from a few to several hundred Kelvin.

We use 41 m baselines between unit telescopes to effectively single out and analyse the inner disc emission. With a suite of shorter, 15 m baselines between pairs of auxiliary telescopes, we probe the transition region between the gap and the outer disc, and beyond. To derive most robust constraints on the radial mid-infrared brightness profile, we make very basic assumptions of black-body emission from featureless dust, and a vertically thin, axially symmetric gapped disc model. We take full advantage of some of the observationally constrained parameters from the prior literature, such as the location of the inner rim (VLTI/AMBER), location of the wall of the outer disc (VLT/CRIRES, VLT/NACO) and use the physically consistent disc temperatures from sophisticated radiative transfer modelling of the spectral energy distribution of HD 100546, as guidance in our choice of temperature.

Our main conclusions can be summarised as follows:

- *The inner disc extends no further than 0.7 AU from the star.* Contrary to prior SED modelling done assuming an inner disc with a 4 AU radius, our uniquely sensitive data for the first time provide a stringent upper limit of 0.7 AU to the radial distribution of the dust in the inner disc.

- *The gap is about 10 AU wide and free of detectable mid-infrared emission.* Much larger dust, rocks and planetesimals are not efficient N-band emitters and they may well be present in the gap.
- *Our modelling places the radial peak of N-band emission from the outer disc at 11 AU.* This estimate is relatively close to the pronounced peak in ro-vibrational CO line emission observed around 13 AU by van der Plas et al. (2009) and the bright ring of polarised light shown in Quanz et al. (2011).
- *The 7.7  $\mu\text{m}$  and 8.6  $\mu\text{m}$  PAH features come from the outer disc.* Absent from our total flux measurements with unit and auxiliary telescopes, these features arise from an angle larger than the slit of our telescopes. On spatial scales, this corresponds to about 100 AU from the star.
- *The inner disc is asymmetric.* Our identical long baselines successfully single out the emission from the inner disc and show variability in the correlated fluxes. Combined with the clear and strong deviations from zero in the chromatic phases in all our UT measurements, this is a direct evidence of asymmetry. Asymmetry persisted over the 1.5 year period.
- *The disc wall is symmetric.* The chromatic phases in our AT measurements are fully consistent with an axially symmetric brightness distribution.

The data we present answers several questions, but also opens an avenue for further investigation. Is the asymmetric spatial distribution of dust in the inner disc long-lived? Follow-up observations on similar baselines with MIDI can answer this. In case of a long-lived resonant asymmetric structure, how exactly is the dust distributed azimuthally? Future VLTI instrument MATISSE and VLT instrument SPHERE will be in the position to directly image the inner disc, and point to the origin of the resonance. Also, further observations with MIDI using pairs of auxiliary telescopes, and especially in the future with hybrid baselines between the unit and auxiliary telescopes, will allow a far better uv-coverage and fidelity, essential to map the wall of the outer disc with MIDI. One of the key standing questions is: Does the inner disc possess sufficient amounts of gas to be viscous and in hydrostatic equilibrium, or has it already evolved to a debris disc stage, in which the dust is large, on Keplerian orbits, and grinds collisionally to produce the small dust that we observe? If so, HD 100546 would be the first known star to be surrounded by both debris disc in the inner regions and an optically thick disc in the outer regions.

**Acknowledgements.** The research of O. P. leading to these results has received funding from the European Community's Seventh Framework Programme (FP7/2007-2013/) under grant agreement No 229517. O. P. wishes to thank the Max Planck Institute for Astronomy in Heidelberg for the research grant awarded in 2011, which was used for this project. G.D.M. acknowledges support from the Leids Kerkhoven-Bosscha Fonds. The authors thank A. Verhoeff, B. Acke and C. Leinert for sharing their previous data, L.B.F.M. Waters, C. A. Hummel for advice and discussions.

## References

- Acke, B. & van den Ancker, M. E. 2004, A&A, 426, 151
- Acke, B. & van den Ancker, M. E. 2006, A&A, 449, 267
- Andrews, S. M., Wilner, D. J., Espaillat, C., et al. 2011, ApJ, 732, 42
- Ardila, D. R., Golimowski, D. A., Krist, J. E., et al. 2007, ApJ, 665, 512
- Augereau, J. C., Lagrange, A. M., Mouillet, D., & Ménard, F. 2001, A&A, 365, 78
- Benisty, M., Tatulli, E., Ménard, F., & Swain, M. R. 2010, A&A, 511, A75
- Bouwman, J., de Koter, A., Dominik, C., & Waters, L. B. F. M. 2003, A&A, 401, 577
- Brown, J. M., Blake, G. A., Dullemond, C. P., et al. 2007, ApJ, 664, L107
- Brown, J. M., Blake, G. A., Qi, C., et al. 2009, ApJ, 704, 496
- Calvet, N., D'Alessio, P., Hartmann, L., et al. 2002, ApJ, 568, 1008

- Cohen, M., Walker, R. G., Carter, B., et al. 1999, *AJ*, 117, 1864
- Crida, A., Morbidelli, A., & Masset, F. 2006, *Icarus*, 181, 587
- di Folco, E., Dutrey, A., Chesneau, O., et al. 2009, *A&A*, 500, 1065
- Espaillet, C., D'Alessio, P., Hernández, J., et al. 2010, *ApJ*, 717, 441
- Glindemann, A., Algomado, J., Amestica, R., et al. 2003, in *ESA Special Publication*, Vol. 522, *GENIE - DARWIN Workshop - Hunting for Planets*
- Goto, M., van der Plas, G., van den Ancker, M., et al. 2012, *A&A*, 539, A81
- Grady, C. A., Woodgate, B., Heap, S. R., et al. 2005a, *ApJ*, 620, 470
- Grady, C. A., Woodgate, B. E., Bowers, C. W., et al. 2005b, *ApJ*, 630, 958
- Guimarães, M. M., Alencar, S. H. P., Corradi, W. J. B., & Vieira, S. L. A. 2006, *A&A*, 457, 581
- Haisch, Jr., K. E., Lada, E. A., & Lada, C. J. 2001, *ApJ*, 553, L153
- Hillenbrand, L. A. 2008, *Physica Scripta Volume T*, 130, 014024
- Jaffe, W. J. 2004, in *Society of Photo-Optical Instrumentation Engineers (SPIE) Conference Series*, Vol. 5491, *Society of Photo-Optical Instrumentation Engineers (SPIE) Conference Series*, ed. W. A. Traub, 715
- Leinert, C. 2003, in *ESA Special Publication*, Vol. 522, *GENIE - DARWIN Workshop - Hunting for Planets*
- Leinert, C., Graser, U., Przygodda, F., et al. 2003, *Ap&SS*, 286, 73
- Leinert, C., van Boekel, R., Waters, L. B. F. M., et al. 2004, *A&A*, 423, 537
- Liu, W. M., Hinz, P. M., Meyer, M. R., et al. 2003, *ApJ*, 598, L111
- Morel, S., Ballester, P., Bauvir, B., et al. 2004, in *Society of Photo-Optical Instrumentation Engineers (SPIE) Conference Series*, Vol. 5491, *Society of Photo-Optical Instrumentation Engineers (SPIE) Conference Series*, ed. W. A. Traub, 1666
- Mulders, G. D., Waters, L. B. F. M., Dominik, C., et al. 2011, *A&A*, 531, A93
- Paardekooper, S.-J. & Mellema, G. 2004, *A&A*, 425, L9
- Panić, O., van Dishoeck, E. F., Hogerheijde, M. R., et al. 2010, *A&A*, 519, A110
- Pantin, E., Waelkens, C., & Lagage, P. O. 2000, *A&A*, 361, L9
- Piétu, V., Dutrey, A., Guilloteau, S., Chapillon, E., & Pety, J. 2006, *A&A*, 460, L43
- Quanz, S. P., Schmid, H. M., Geissler, K., et al. 2011, *ApJ*, 738, 23
- Quillen, A. C. 2006, *ApJ*, 640, 1078
- Ratzka, T. & Leinert, C. 2005, *Astronomische Nachrichten*, 326, 570
- Ratzka, T., Leinert, C., Henning, T., et al. 2007, *A&A*, 471, 173
- Ratzka, T., Leinert, C., van Boekel, R., & Schegerer, A. A. 2009, in *Science with the VLT in the ELT Era*, ed. A. Moorwood, 101
- Tatulli, E., Benisty, M., Ménard, F., et al. 2011, *A&A*, 531, A1
- Thalmann, C., Grady, C. A., Goto, M., et al. 2010, *ApJ*, 718, L87
- van Boekel, R. 2004, PhD thesis, *FNWI: Sterrenkundig Instituut Anton Pannekoek*, Postbus 19268, 1000 GG Amsterdam, The Netherlands
- van Boekel, R., Waters, L. B. F. M., Dominik, C., et al. 2004, *A&A*, 418, 177
- van den Ancker, M. E., The, P. S., Tjin A Djie, H. R. E., et al. 1997, *A&A*, 324, L33
- van der Plas, G., van den Ancker, M. E., Acke, B., et al. 2009, *A&A*, 500, 1137
- van Leeuwen, F., ed. 2007, *Astrophysics and Space Science Library*, Vol. 350, *Hipparcos, the New Reduction of the Raw Data*
- Verhoeff, A. 2009, PhD thesis, *Sterrenkundig Instituut "Anton Pannekoek"*, University of Amsterdam
- Verhoelst, T. 2005, PhD thesis, *Institute of Astronomy, K.U.Leuven, Belgium*